SCIENCE CHINA
Chemistry

•REVIEWS•
SPECIAL ISSUE: 2023 Emerging Investigator Issue

https://doi.org/10.1007/s11426-023-1799-y

Electrifying the future: the advances and opportunities of electrocatalytic carbon dioxide reduction in acid

Runhao Zhang[1,2†], Haoyuan Wang[1,2†], Yuan Ji[3], Qiu Jiang[1,3], Tingting Zheng[3*] & Chuan Xia[1,3*]

[1]*Yangtze Delta Region Institute (Huzhou), University of Electronic Science and Technology of China, Huzhou 313001, China;*
[2]*Hefei National Research Center for Physical Sciences at the Microscale, University of Science and Technology of China, Hefei 230026, China;*
[3]*School of Materials and Energy, University of Electronic Science and Technology of China, Chengdu 611731, China*

Received July 30, 2023; accepted September 7, 2023; published online September 26, 2023

Transforming carbon dioxide (CO_2) into products using renewable electricity is a crucial and captivating quest for a green and circular economy. Compared with commonly used alkali electrolytes, acidic media for electrocatalytic CO_2 reduction (CO_2RR) boasts several advantages, such as high carbon utilization efficiency, high overall energy utilization rate, and low carbonate formation, making it a compelling choice for industrial applications. However, the acidic CO_2RR also struggles with formidable hurdles, encompassing the fierce competition with the hydrogen evolution reaction, the low CO_2 solubility and availability, and the suboptimal performance of catalysts. This review provides a comprehensive overview of the CO_2RR in acidic media. By elucidating the underlying regulatory mechanism, we gain valuable insights into the fundamental principles governing the acidic CO_2RR. Furthermore, we examine cutting-edge strategies aimed at optimizing its performance and the roles of reactor engineering, especially membrane electrode assembly reactors, in facilitating scalable and carbon efficient conversion. Moreover, we present a forward-looking perspective, highlighting the promising prospects of acidic CO_2RR research in ushering us towards a carbon-neutral society.

electrocatalytic CO_2 reduction, acidic electrolyte, microenvironment, alkali metal cations, electrolysers

Citation: Zhang R, Wang H, Ji Y, Jiang Q, Zheng T, Xia C. Electrifying the future: the advances and opportunities of electrocatalytic carbon dioxide reduction in acid. *Sci China Chem*, 2023, 66, https://doi.org/10.1007/s11426-023-1799-y

1 Introduction

The rapid increase in atmospheric carbon dioxide (CO_2) levels due to the extensive utilization of fossil fuels poses a serious threat to the global environment and climate [1]. A promising way to tackle this challenge is the electrochemical reduction of CO_2 (CO_2RR), which can not only remove CO_2 from the air but also turn it into valuable fuels or chemical feedstocks [2–6], such as carbon monoxide (CO) [2], formic acid (HCOOH) [3], methane (CH_4) [4], ethylene (C_2H_4) [5], and ethanol (C_2H_5OH) [6], using renewable electricity. This multifaceted strategy of CO_2RR holds a dual advantage, encompassing the mitigation of CO_2 emissions and the establishment of a sustainable avenue for storing renewable energy in the form of chemical bonds [7]. By turning CO_2 into useful products, CO_2RR can harmonize the variable nature of renewable energy sources, such as solar and wind, by offering flexible and on-demand chemical production, and opens up new opportunities for the green chemical industry and energy sector.

The performance of the CO_2RR is highly dependent on the choice of the electrolyte, which is profoundly impacted by key factors such as CO_2 solubility, pH at the electrode surface, ion transport, and catalyst stability. Currently, most of the reported CO_2RR studies have used alkali electrolytes, which offer some advantages including high CO_2 solubility, low overpotential, and facile hydroxide ion supply [8,9].

†These authors contributed equally to this work.
*Corresponding authors (email: ttzheng@uestc.edu.cn; chuan.xia@uestc.edu.cn)

However, alkali electrolytes also pose significant challenges for efficient and stable CO_2RR [10]. In alkali electrolytes, CO_2 readily reacts with OH^- in the electrolyte to form HCO_3^- or CO_3^{2-}, which lowers the overall single path conversion efficiency (SPCE) [11]. Despite efforts to enhance the SPCE, such as the approach proposed by Wang *et al*. [12], involving the use of a porous solid electrolyte layer containing sulfuric acid groups between the cathode and anode to facilitate the neutralization of carbonate ions and protons to generate CO_2 gas, the stability and conductivity issues of solid-state electrolytes remain quite challenging. Moreover, over 50% of the energy input is used for carbon regeneration, further reducing the energy utilization efficiency [13]. Additionally, the potential high salt concentration in localized areas can lead to the precipitation on the cathode, causing the blockage in the gas diffusion electrode (GDE) microchannels and increasing the cell resistance. Such complications are further exacerbated at elevated current densities (>1 A cm^{-2}) [14], a parameter of considerable importance for industrial-scale applications. Therefore, it is essential to develop alternative electrolytes that can overcome the limitations of alkali electrolytes for the CO_2RR.

Acidic electrolytes have emerged as a promising alternative for CO_2RR, as they provide ample protons for CO_2 hydrogenation without consuming water, thereby improving the energy efficiency and avoiding water depletion [15]. In acidic media, the higher local concentration of H^+ significantly suppresses the formation of (bi)carbonate species, resulting in an increase of the SPCE and energy utilization efficiency of the CO_2RR process (Table 1) [16].

Even in the case of H_2O serving as the proton source, any carbonate formed locally will be converted back to CO_2 by protons in the bulk electrolyte. This makes acidic media an attractive option for minimizing carbonate formation and eliminating CO_2 crossover, which is beneficial for industrial applications. However, achieving the high selectivity and activity for CO_2RR in acidic media is difficult due to the dominance of the hydrogen evolution reaction (HER) as a result of high proton concentrations [21]. In this regard, advancing the CO_2RR in acidic media is crucial to surmount the hurdle of competitive HER while achieving high carbon utilization efficiency (Figure 1).

So far, the mechanism of CO_2 electroreduction in acid remains intricate and has not been fully elucidated [22–24]. Due to the abundance of protons in acidic media, it is crucial to grasp and regulate the rivalry between the HER and CO_2RR. One major determinant of the outcome of this competition, in additional to the inherent properties of catalysts, is their microenvironment [25]. The microenvironment of the catalyst can be associated with the alkali metal cation type and concentration and the local pH, among others. It has been revealed that alkali metal cations can modulate several aspects of the acidic CO_2RR, such as the interfacial electric field, the adsorption strength of CO_2 and its intermediates, and the concentration profiles of CO_2 and H^+ at the electrode surface [26–28]. The local pH can also have profound impacts on the CO_2RR performance, which can be either beneficial or detrimental, depending on the catalyst type, structure and electrolyte composition [29]. However, the alkali effects are not isolated from but rather intertwined with local pH, making it difficult to disentangle and quantify their individual roles. Therefore, it is essential to unravel the mechanism and optimize the microenvironment of catalysts for acidic CO_2RR.

To boost the performance of the CO_2RR in acidic electrolytes, several strategies have been pursued until now [30]. One approach is to devise new acid-resistant and efficient catalysts that can surmount the high overpotential and HER competition in acidic media. These catalysts are expected to enable facile electron transfer and possess appropriate binding energy of each intermediate for target products [31]. Another key strategy is the regulation of the microenvironment by structure engineering and surface modification of catalysts, which can manipulate the interfacial properties and reaction pathways [30]. Specifically, structure engineering can tailor the morphology, size, porosity, and surface area of catalysts, impacting CO_2 adsorption, mass transport, and electron transfer. Surface modification can affect CO_2 activation, intermediate stabilization, and product desorption by changing the charge, wettability, and functional groups of catalysts. Equally important is reactor engineering which drives the advancement of the performance and scalability of acidic CO_2RR. In particular, membrane electrode assembly (MEA) reactors featuring a compact and modular structure have been delicately engineered for carbon-efficient CO_2RR in acid [32].

Table 1 Corresponding SPCE values in different media

Product	Media	FE_{CO_2RR} (%)	$SPCE_{CO_2RR}$ (%)
CO	0.5 mol L^{-1} K_2SO_4, pH=1.1	95	46.2 [17]
	1 mol L^{-1} KOH, pH=13.7	>90	<10 [17]
C_{2+}	2.5 mol L^{-1} KCl, pH≈1	90	60 [16]
	0.5 mol L^{-1} K_2SO_4, pH=2	88	60 [18]
	0.1 mol L^{-1} $KHCO_3$, neutral	49	35.5 [19]
	1 mol L^{-1} KOH, pH=13.7	93	14 [20]

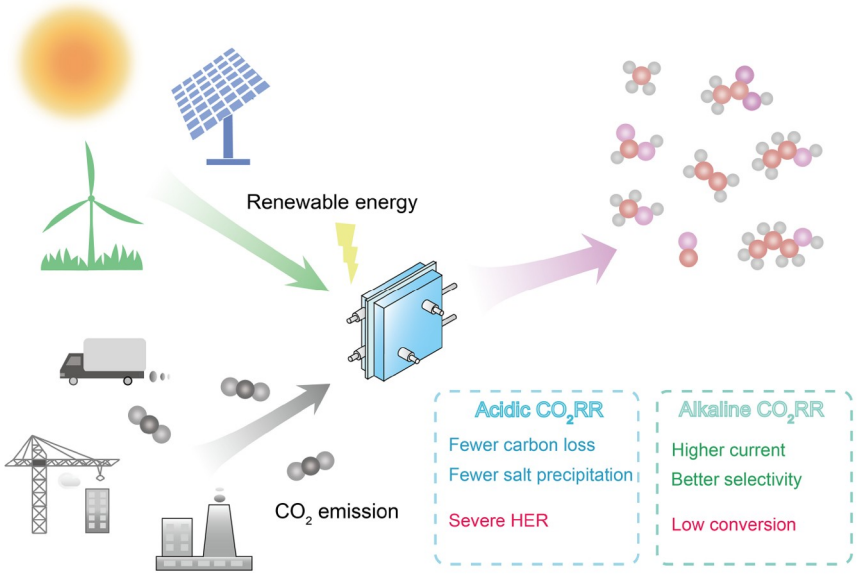

Figure 1 Schematic illustration of CO_2 upcycling *via* an electrolyzer powered by renewable energy. For a CO_2 electrolyzer, acidic electrolytes boast several advantages with the high carbon utilization, energy efficiency, and low carbonate formation (color online).

The aim of this review is to offer a comprehensive overview of the recent progress and challenges in electrocatalytic CO_2 reduction in acidic media. We start by discussing the basic regulatory mechanism of the CO_2RR in acid, which involves the rivalry between the HER and CO_2RR and the effect of alkali metal cations. Strategies to enhance acidic CO_2RR activity, such as manipulating intermediates, catalyst morphology, and surface modification, are reviewed in detail, along with their effects on interfacial properties and reaction pathways. We also spotlight the roles of reactor engineering in facilitating acidic CO_2RR, with a special emphasis on MEA reactors, and their versatile potential for scalable and carbon-efficient CO_2RR. This review concludes with some perspectives and future directions for acidic CO_2RR research, aiming to spark more research efforts in developing efficient and scalable acidic CO_2RR systems towards a carbon-neutral society.

2 Theory-guided CO_2RR in acidic media

Generally, the catalytic reduction of CO_2 at the electrode/electrolyte interface involves the following steps [33]: (1) CO_2 adsorption on the active sites of the surface, which determines the initial orientation and activation of the molecule; (2) sequential or coupled proton and electron transfer leading to the reduction of CO_2 to crucial adsorbed intermediate species, such as $*CO_2^-$, *COOH, *CO and $*CH_3O$, by either forming O–H, breaking C=O, or forming C–H bonds, which governs the reaction pathway and kinetics; (3) possible interactive coupling of intermediate species, which affects the product distribution and selectivity and (4) desorption of the final products, which impacts the catalyst efficiency and stability. By and large, the electrocatalytic processes occurring over the cathodes are highly complex and influenced by various factors, such as catalyst structure and composition, applied potential, electrolyte type and concentration and pH as well as mass transport. Table 2 summarizes the half electrochemical thermodynamic reactions on the cathodes during the aqueous CO_2RR [34]. At present, the most direct way that enhances the intrinsic activity of catalysts towards CO_2RR is to tune the electronic properties of catalysts, such as the *d*-band centers, work function and charge density [35]. By doing so, the binding energy of each intermediate in the conversion mechanism can be ingeniously controlled. The optimal binding energy should be neither too strong nor too weak, following the Sabatier principle [36]. The accumulation of CO_2RR intermediates would occupy available active sites and in turn suppress other undesired byproduct paths, leading to the high selectivity of CO_2RR. On the other hand, accelerating the electron transfer to CO_2 molecules can lower the activation barrier in most CO_2RRs. This can be achieved by introducing defects, dopants or heteroatoms into the catalysts to create more active sites or modify their electronic structure [37].

One of the major challenges of the CO_2RR in acidic media is fierce competition with the HER, which significantly compromises the Faradaic efficiency and energy efficiency of the desired products. Therefore, a key strategy for achieving high-performance CO_2RR under acidic conditions is to suppress the HER or enhance the CO_2RR by manipulating the catalyst properties or its microenvironment. The latter is closely related to the effect of alkali metal cations, which can influence various aspects of the reaction micro-

Table 2 Half electrochemical thermodynamic reactions of CO_2RR, together with their corresponding standard redox potentials (*versus* reversible hydrogen electrode (RHE))

Product	Reaction	E^0 (V) *vs.* RHE
CO	$CO_2+2H^++2e^-\rightarrow CO(g)+H_2O$	−0.11
HCOOH	$CO_2+2H^++2e^-\rightarrow HCOOH(aq)$	−0.12
CH_3OH	$CO_2+6H^++6e^-\rightarrow CH_3OH(aq)+H_2O$	0.03
CH_4	$CO_2+8H^++8e^-\rightarrow CH_4(g)+2H_2O$	0.17
C_2H_4	$2CO_2+12H^++12e^-\rightarrow C_2H_4(g)+4H_2O$	0.08
C_2H_5OH	$2CO_2+12H^++12e^-\rightarrow C_2H_5OH(aq)+3H_2O$	0.09

environment and the reaction kinetics. To unravel the competitive mechanisms between the two reactions and the regulatory mechanisms of alkali-metal cations, it is imperative to identify the discharge sequence of each species in the overall reaction process and elucidate their interactions with the catalyst surface. Only by doing so, can we provide clear guidance for designing catalysts that can selectively bind CO_2 over H^+ and facilitate the formation of CO_2RR intermediates.

2.1 Competition between HER and CO_2RR

The high concentration of H^+ in acidic media is the main culprit for the competitive HER which hinders the efficient CO_2RR in acidic media. The excess of H^+ reduces the thermodynamic potential for the HER, making it more favorable than the CO_2RR at low overpotentials. Therefore, to enhance the efficiency of the CO_2RR under acidic conditions, it is crucial to understand and manipulate the competitive relationship between the HER and CO_2RR. Broekmann *et al.* [22] first used an Ag inverted rotating disk electrode (pH=4.17, 0.1 mol L^{-1} K_2SO_4 with saturated CO_2) to analyze the discharge sequence of species in a non-strong acidic system, which was found to be: H^+ (1.2–1.4 V *vs.* Ag|AgCl) >CO_2 (−1.6 V *vs.* Ag|AgCl) > H_2O (−1.8 V *vs.* Ag|AgCl). Building upon these findings, Ooka *et al.* [23] observed a decrease in the water reduction current upon the saturation of CO_2 or CO on a polycrystalline Cu rotating disk electrode (pH=2.5, 0.1 mol L^{-1} $NaClO_4$). However, the H^+ discharge exhibited a plateau current and remained unaffected. Differential electrochemical mass spectrometry (DEMS) data further supported the proximity of the peak current potential for H_2 and the starting potential for CO, thus confirming the inhibition of water reduction HER by CO_2RR [24].

The process of CO_2 reduction in non-strongly acidic media can be preliminarily summarized as follows [22–24]: the reaction starts with H^+ at a relatively lower potential, and as the potential increases, H^+ gradually reaches the diffusion limit, leading to a surface pH ⩾ 7 at the electrode:

$2H^++2e^-\rightarrow H_2$

Subsequently, the reduction of CO_2 is initiated. The H_2O acts as the hydrogen donor and the generated OH^- can consume the H^+ brought by the diffusion. The intermediate CO adsorbs at the active sites, inhibiting the formation of H* species, thereby suppressing the overall HER activity. This leads to an increase in the Faradaic efficiency of the CO_2RR:

$*+CO_2+H_2O+e^-\rightarrow *COOH+OH^-$

$*COOH+e^-\rightarrow *CO+OH^-$

$OH^-+H^+\rightarrow H_2O$

However, when the potential becomes sufficiently high, the discharge of H_2O will increase, and the generated OH^- will react with CO_2 to form the (bi)carbonate, reducing the surface gas partial pressure. Consequently, this leads to a decrease in FE_{CO_2RR}.

$2H_2O+2e^-\rightarrow H_2+2OH^-$

$OH^-+CO_2\rightarrow HCO_3^-$

It is worth noting that the above discussion pertains to non-strongly acidic systems. Although the CO_2RR mechanisms are similar in different media, acidic CO_2RR faces a unique challenge of competing with the HER, resulting in a low selectivity for CO_2RR. For strongly acidic systems (bulk phase pH⩽1), even at high current densities, the electrode surface may still remain in an acidic environment. H^+ could potentially serve as a direct source of protons. Xie *et al.* [18] utilized COMSOL to simulate the pH at the electrode interface and found that when the bulk pH is less than 1, even at a current density of 500 mA cm^{-2}, the electrode vicinity (0–100 μm) remains significantly acidic (Figure 2a). Clearly, under such conditions, the CO_2RR fails to outcompete the HER. There is considerable room for the improvement in the performance of the CO_2RR under strongly acidic conditions, and hence, we believe that this is a promising direction for the future development. To ensure a favorable microenvironment for the CO_2RR on the electrode surface, it can be achieved by adjusting the current density and bulk phase pH. Applying a higher current density ensures sufficient generation of OH^- to counterbalance H^+, but it should not be excessively high as it would still lead to CO_2 consumption. However, altering the pH should be done with the caution as it may result in the changes in product selectivity, achieved through altering the coupling or sequence of proton and electron transfers. For products with pH-dependent reaction rates, such as methane, a lower pH is more favorable for the CPET hydrogenation of *CO, thus promoting CH_4 forma-

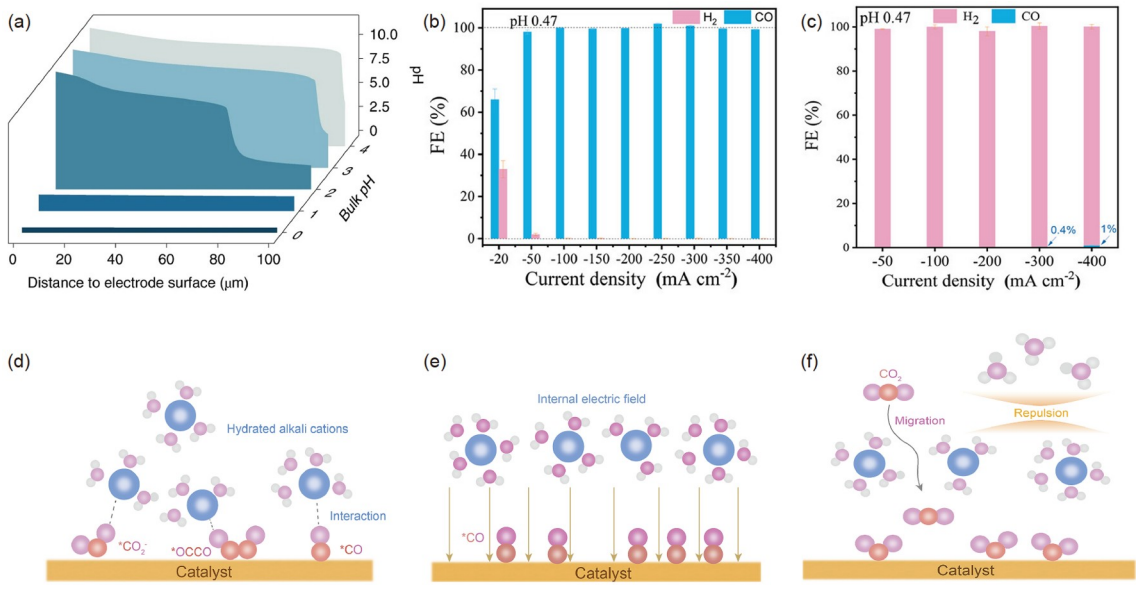

Figure 2 (a) Modeled pH changes along the catalyst surface in solution at different pH values under an applied current density of 500 mA cm^{-2} and the relationship between surface pH at varying applied current densities and bulk pH. Reproduced with permission from [18]. Copyright 2022 Springer Nature. (b) FEs of H_2 and CO for NiPc-OMe in 0.1 mol L^{-1} H_2SO_4+0.4 mol L^{-1} K_2SO_4 when K_2SO_4 was eliminated in (c), indicating the effectiveness of the electrolyte K^+ effect for the acidic CO_2RR. Reproduced with permission from [39]. Copyright 2022 John Wiley and Sons. (d) Cation effect stabilizing key intermediates during the acidic CO_2RR. (e) Cation effect enhancing local internal electric field among the surface. (f) Cation effect repulsing the transport of hydronium ions (color online).

tion. On the other hand, for products where the rate-determining step is independent of H^+ concentration, such as CO, the selectivity will decrease [38].

2.2 The effect of alkali metal cations

A noteworthy feature of the experiments discussed in Section 2.1 is that they all involve the participation of alkali metal cations (such as K^+ and Na^+). This is because in acidic systems devoid of alkali metal cations, the products of the CO_2RR are barely detectable. In a pH=3 medium without alkali metal cations, neither Cu nor Ag electrodes exhibit the CO_2RR activity [26]. As the concentration of alkali cations increases, the production of CO through CO_2RR increases proportionally until reaching a maximum. In a more acidic environment (pH=0.47), β-tetramethoxy-substituted nickel phthalocyanine (NiPc-OMe), which was immobilized on multi-walled carbon nanotubes (CNTs), exhibits a remarkable increase in the FE_{CO} from almost 0% to nearly 100% upon the introduction of 0.8 mol L^{-1} K^+ (Figure 2b and 2c) [39]. These results provide the compelling evidence for the significant role of alkali metal ions in enhancing CO_2RR activity.

According to the latest studies in the field, the influence of alkali metal cations on the properties and behavior of acidic solutions can be explained by three main factors (Figure 2d and 2f).

Interaction with reaction intermediates. The interaction with reaction intermediates can be understood from two aspects: the stabilization of intermediates and the reduction of the CO_2RR activation energy barrier. For charged intermediates such as CO_2^-, alkali metal cations stabilize them through short-range electrostatic interactions, as well as medium-range interactions with the induced electric field generated by the cations in the solvent. DFT calculations have confirmed that the introduction of alkali metal cations can lower the formation energy of CO_2^- by approximately 0.5 eV [26]. In the case of neutral intermediates, such as *CO and *OCCO, dipolar-polarizable molecules are stabilized by the interface electric field induced by the cations [40]. The stabilization energy (ΔE) can be described by the following equation, which is related to the dipole moment (μ), polarizability (α), and induced electric field strength (ε):

$$\Delta E=\mu\varepsilon-1/2\alpha\varepsilon^2$$

Thus, this stabilization effect will also influence the selectivity of the products. For smaller solvated metal ions (*e.g.*, K^+, Cs^+), a larger induced electric field is generated, leading to the higher stability for larger dipolar species (*OCCO) compared with smaller dipolar species (*CO). Consequently, the activation energy for the C–C coupling is reduced [41]. Therefore, it can be observed that as the ratio of electrolyte K^+/Na^+ gradually increases, the selectivity for C_1 products decreases, corresponding to an increase in $FE_{C_{2+}}$ [42]. Alkali metal cations also reduce the activation barriers of the CO_2RR. The coordination of CO_2^- by these cations can lower the O–C–O bond angle and enhance the electron transfer to CO_2^- at the electrode. Larger cations possess softer solvation shells, making it easier for CO_2^- inter-

mediates to coordinate with them. According to AIMD simulations, the coordination numbers of alkali metals with O in CO_2 are as follows: $N_{Li-O(CO_2)}$=0.1±0.3<$N_{Na-O(CO_2)}$ = 0.9 ±0.2<$N_{K-O(CO_2)}$=0.9±0.4<$N_{Cs-O(CO_2)}$=1.3±0.5. Consequently, the activity of the CO_2RR increases in the order Li<-Na<K<Cs [26].

Increase the internal electric field intensity (ε) of the Stern layer [27,28]. According to Gauss's flux theorem, ε is determined by the surface excess charge density. In an acidic solution without alkali metal cations, the electrode potential (φ_M) moves in the negative direction, and the potential at the outer Helmholtz plane (φ_{OHP}) moves with the same magnitude. Since H^+ is the main species responsible for the surface excess charge at the OHP, the surface excess charge density remains constant, by considering the combined effects of its generation and consumption during the HER. However, the introduction of alkali metal cations allows more unreactive metal cations to accumulate near the OHP under a more negative φ_M, resulting in a smaller amplitude of φ_{OHP} movement and an increased value of ε. This enhancement effect increases with a decrease in the hydrated radius of the cation (Li^+>Na^+>K^+~Cs^+) due to reduced steric hindrance and electrostatic repulsion between cations, leading to increased cation concentration at the OHP. The electric field in the Stern layer also stabilizes intermediates and enhances the CO_2RR current.

Inhibit HER induced by H^+ at low potentials. In acidic media on Au electrodes, the plateau current for H^+ discharge decreases with increasing alkali metal cation concentration, irrespective of the cation type [27,28] because alkali metal cations adsorbed at the OHP generate a reverse electric field in the diffusion layer that inhibits H^+ diffusion. Furthermore, according to Qin *et al*. [28], the expression for the current density of H^+ migration in the HER is given by:

$$j_{H^+,mig} = -D_{H^+}F\left(\frac{dC_{H^+}}{dx} + 2\frac{dC_{M^+}}{dx}\right)$$

Since $dC_{M+}/dx < 0$, the HER is weakened. Under mildly acidic conditions, the limiting current density for H^+ reduction is insensitive to the characteristics of the electrode–electrolyte interface, and the influence of ion species can be neglected. However, the concentration of alkali metal cations should not be excessively high, as an increase in local pH under high current conditions can lead to the salt precipitation, thereby diminishing the catalyst's activity.

It is worth noting that metal cations also promote the water discharge at higher potentials, and the influence of alkali metal cations on the alkali HER has been extensively discussed [43,44]. As the charge density of the metal cation increases, the electrons in the oxygen of water molecules are further attracted to the metal center, weakening the hydrogen bonds of water molecules and reducing the barrier for water dissociation. Therefore, for high charge density metal cations such as Nd^{3+} and Ce^{3+}, although the interaction strength with CO_2RR intermediates is further enhanced and the surface electron density is increased, this promotion of the CO_2RR can only be observed at low potentials, as their promotion of the HER is stronger at high potentials [45].

3 Strategies to boost the efficiency of acidic CO_2RR

Despite the urgent need for effective acidic CO_2 conversion into value-added products, the current research in this field remains insufficient and unsatisfactory. To provide a comprehensive and systematic understanding of this challenging topic, this review focuses on revealing the intricate interplay between the structure and properties of catalysts and the regulatory mechanism of the acidic CO_2RR. In the Section 2, we pinpointed three crucial factors that can significantly boost the efficiency of acidic CO_2RR: fine-tuning the formation barrier or binding energy of key intermediates to enhance the intrinsic activity of the catalyst and suppress the competing HER; elevating the local concentration of alkali metal cations and CO_2 at the electrode interface by engineering sophisticated microenvironments; and increasing the local pH to create favorable conditions for CO_2RR, for instance, by restricting the diffusion of OH^- and diminishing the mass transfer of H^+. For leveraging these regulatory mechanisms, we will in this section delve into the intricate interplay between the catalyst properties and the reaction mechanisms by showcasing some recent advances in acidic CO_2RR that demonstrate novel and effective regulation strategies and methods.

3.1 Fine-tuning the formation of intermediates

At the microscopic level, the formation rate and thermodynamic stability of key intermediates on the catalysts are vital for boosting the reaction activity of the CO_2RR [46]. Regarding the formation rate, some intermediates, such as *CO, are generated on catalysts through a pivotal step involving proton-decoupled electron transfer to produce $*CO_2^-$, leading to a reaction rate that remains invariant with changes in pH (electrode potential *vs*. NHE). Conversely, the generation of H_2 on catalysts increases with decreasing pH (electrode potential *vs*. NHE) [47]. Therefore, it is imperative to lower the activation energy for *CO generation on catalysts to ensure a high reaction rate, and this can be accomplished by enhancing the electron transfer to form $*CO_2^-$. From the standpoint of thermodynamic stability, it is more desirable if the adsorption energy of intermediates on catalysts is much higher than that of *H [48]. Thus, it is worth exploring the engineering of sites on catalysts with weak *H adsorption but strong adsorption for CO_2RR intermediates.

3.1.1 *Accelerating the electron transfer*

To tackle the sluggish step in acidic electrolytes, new materials and electrolytic systems can be delicately investigated to enhance the electron transfer, which is a key factor for improving the formation rate and thermodynamic stability of CO_2RR intermediates. For example, Wang *et al*. [49] synthesized a novel $Cs_3Bi_2Br_6$ perovskite material and mixed it with XC-72 to obtain a $Cs_3Bi_2Br_6$/C catalyst. In a flow cell with a medium of 3 mmol L^{-1} HBr+0.5 mol L^{-1} CsBr (pH=2.5), the catalyst maintained a formic acid partial current density of 133.7 mA cm^{-2} (close to 90% Faradaic efficiency) and 47.2% SPCE (1.45 V *vs*. RHE) for 10 h. With the assistance of the *in-situ* ATR-SEIRA spectra presented in Figure 3a, the mechanism study shows that the peak assigned to $*CO_2^-$ is strengthened with increasing potential. The evidenced accumulating radical species demonstrate that the initial electron transfer is not the rate-determining step, but accelerates the CO_2 conversion rate. It is proposed that the surface metal ions act as stabilizers for the generated $*CO_2^-$ species, which subsequently react with the proton to form OCHO* inhibiting the HER process. Tafel plots and DFT calculations also indicated a lower reaction barrier for the rate-determining step (*OCHO formation) on $Cs_3Bi_2Br_6$/C, which is significantly smaller than that of the HER, revealing the origin of its high activity.

Catalysts with isolated sites offer another solution for this decoupled electron-proton transfer process. The most commonly used isolated-site catalysts are M–N–C (M=Co, Fe, Mn, Cu, Ni), which proceed with the smallest overpotential for CO_2 reduction and sluggish hydrogen evolution process [50,51]. For example, Gonglach *et al*. [52] developed a Co(III) corrole molecular complex (Figure 3b) and immobilized it on carbon paper to prepare an electrode. The electron-rich square planar Co(I) active center formed during the electroreduction is crucial for the CO_2RR. The electronic paramagnetic resonance experiment after the electrolysis proves the formation of Co (III)–$*CO_2^-$ species. In this work, the high barrier of $*CO_2^-$ formation was notably reduced from −1.5 V to −0.8 V *vs*. RHE. Due to the peculiar electronic properties and coordination configuration, the formed intermediates are readily converted to HCO* for the dimerization step. Consequently, the ethanol selectivity can reach 48% and be maintained for 5 h at 0.8 V *vs*. RHE at pH=6. Later, this group developed a Mn(III) corrole molecular catalyst with a similar structure [53]. The high Lewis acidity of Mn(III) facilitates its preferential binding to the basic O-site rather than the C-site, promoting the formation of oxalate-type intermediates and achieving a 63% Faradaic efficiency for acetic acid in a phosphate buffer system at pH=6.

In addition to classical SACs, diatomic site catalysts exhibit the superior performance in acidic media. Introducing adjacent metal sites can tune the electronic properties of the Ni sites accounting for the exceptional performance. Zhang *et al*. [54] designed a Ni–Cu bimetallic catalyst supported on hollow nitrogen-doped carbon. Extended X-ray absorption fine structure (EXAFS) data at the operating potential indicated that the coordination number of Ni–N/C and Ni–N–O is significantly higher than that before the reaction, sug-

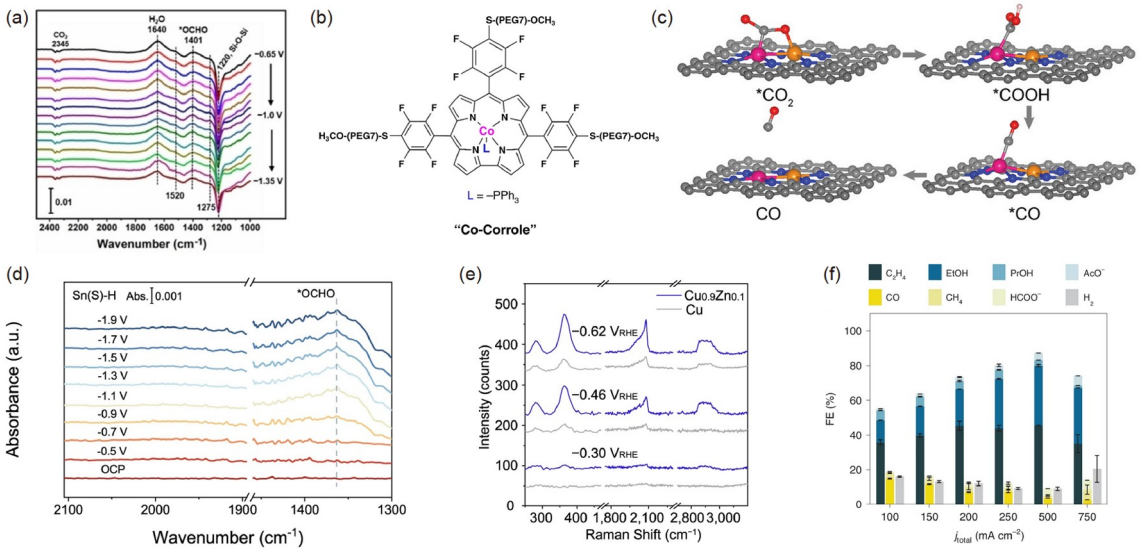

Figure 3 (a) *In-situ* ATR-SEIRA spectra on $Cs_3Bi_2Br_9$/C electrodes in CO_2-saturated 3 mmol L^{-1} HBr electrolyte with 0.5 mol L^{-1} CsBr using a single-beam spectrum taken at −0.3 V *vs*. RHE as the reference. Reproduced with permission from [49]. Copyright 2022 John Wiley and Sons. (b) Chemical structure of the Co-corrole molecule. Reproduced with permission from [52]. Copyright 2019 Springer Nature. (c) The catalytic pathway on NiN_3–CuN_3 *via* $*CO_2^-$ intermediates after optimization. The pink, orange, blue, red, black, and gray spheres represent Ni, Cu, N, O, C, and H atoms, respectively. Reproduced with permission from [54]. Copyright 2023 John Wiley and Sons. (d) *In-situ* ATR-FTIR spectra of S-doped Sn at various potentials. Reproduced with permission from [57]. Copyright 2023 Springer Nature. (e) *In-situ* Raman peaks at 250–470, 1,750–2,300 cm^{-1} and 2,700–3,200 cm^{-1}, indicating the increasing intensity of *CO among $Cu_{0.9}Zn_{0.1}$ catalysts. Reproduced with permission from [58]. Copyright 2023 Springer Nature. (f) FE values of all products on Pd–Cu catalysts under different applied current densities. Reproduced with permission from [18]. Copyright 2022 Springer Nature (color online).

gesting that Ni serves as the active center for the reaction, while Cu acts as a modifier. Bard charge analysis and ESP plots indicated the electron transfer from Cu to Ni, resulting in the Ni in NiN_3–CuN_3 having a *d*-band center (−1.64 eV) closer to the Fermi level compared with Ni (−2.10 eV) in NiN_3, facilitating the adsorption of reactants on the catalyst surface. The formation of $*CO_2^-$ species and consecutive protonation were proposed by DFT calculations, which demonstrated that NiN_3–CuN_3 has a lower rate-determining step ($*CO_2^-$→*COOH) and CO desorption barriers, as well as a higher HER barrier (Figure 3c). In a phosphate buffer electrolyte flow cell at pH=3, the Faradaic efficiency and current density of CO reached 98.5% and 190±11 mA cm^{-2}, respectively, along with the long-term stability.

3.1.2 Manipulating the adsorption of intermediates

Another crucial aspect for promoting the generation of key intermediates is to manipulate the adsorption of the intermediates on the catalyst surface. The adsorption energy of the intermediates dictates the thermodynamic feasibility and the reaction pathway of the CO_2RR. Ideally, the catalyst should have a moderate adsorption energy for the intermediates, neither too strong nor too weak, to prevent the poisoning or desorption of the intermediates. Furthermore, the catalyst should have a selective adsorption for the desired intermediates over the undesired intermediates, such as *H, to inhibit competing reactions while favoring the CO_2RR.

Taking Sn, Bi and Pb catalysts as illustrative examples, these metals share similar high overpotentials toward the HER, which means that they are less likely to be plagued by the competitive HER that would lower the CO_2RR performance [55]. Therefore, catalyst designs based on these main-group metals are widely studied for acidic CO_2RRs and show the tantalizing potential for obtaining desired products under this challenging reaction conditions. For example, since Bi-based catalysts generally have ultra-high HER overpotential, the ultra-thin Bi nanosheets have been experimentally demonstrated to possess the excellent selectivity toward HCOOH in alkali media, and they also exhibit remarkable performance in acidic environments [56]. Qiao and his co-operators [57] developed a highly efficient S-doped Sn electrode generated *in-situ* from the π-SnS electrolytic evolution. The as-synthesized S-doped Sn exhibits a large Tafel slope in Ar-saturated electrolytes, indicating an intrinsically slow dynamic HER process, which is further proven by calculating the *H adsorption free energy in the theoretical model. Figure 3d based on *in-situ* Fourier transform infrared absorption spectra reveals that the accumulation of *OCHO species competes with *H to mitigate HER byproducts. Finally, they achieved almost 92% FE toward formic acid and 36% carbon efficiency at 1 A cm^{-2} (electrolyte pH=3). In addition to the main-group metals, Cu-based catalysts toward hydrocarbons have also been studied. Generally, based on the competitive adsorption of co-adsorbates, sites with strong CO adsorption are believed to have weaker binding energies with *H, resulting in lower HER activity, making them potential candidates for excellent acidic media catalysts. As a universal strategy, introducing other doping elements to modulate Cu electronic properties is a feasible way to solve this problem. Zhang *et al*. [58] fabricated Zn–Cu catalysts to generate asymmetric CO adsorption sites for the lower *CO dimerization barrier. As shown by *in-situ* Raman spectra, the formation of Cu–Zn sites remarkably boosts CO vibration bands at 1,900–2,100 cm^{-1}, indicating elevated CO adsorption (Figure 3e). The suppression of the HER by the CO_2RR process resulted in a 69% FE toward C_{2+} products at pH 4. Similarly, Xie *et al*. [18] constructed a series of bimetallic X–Cu catalysts to enhance the affinity toward *CO. They found that Pd–Cu catalysts strongly adsorbed CO_2RR reaction intermediates covering the catalyst surface and occupied the vacant active sites for the HER. Under acidic media (pH=2.0), they successfully achieved almost 90% C_{2+} selectivity and HER lower than 10% as indicated by Figure 3f. Due to the application of the acidic electrolytes, an ultra-high SPCE of 68% in single-pass CO_2 flow proves the efficiency of the acidic CO_2RR.

3.2 Regulating the microenvironment of catalysts

The microenvironment surrounding the catalytic active sites can be modulated by various factors, such as the formation of the solid–gas–liquid three-phase interface, the pH and the ratio of CO_2 to H_2O concentration near the active sites, and the type of cations, which has been confirmed as a universal strategy for enhancing the activity and selectivity of the CO_2RR [59]. In acidic media, the high concentration of H^+ ions at the electrode surface becomes a crucial factor inhibiting the efficient CO_2RR. As described in the Section 2, increasing the concentration of OH^-, alkali metal cations and CO_2 in the local microenvironment is a vital strategy for enhancing CO_2RR performance. The regulation of the local microenvironment may entail controlling the mass transfer of key species (slowing the diffusion of H^+ toward the active sites while localizing OH^- and metal cations at the active site surface) and adjusting the catalyst's optimal hydrophobicity to capture more CO_2. To achieve this goal, we can employ two approaches that can manipulate the local conditions from both microscopic and macroscopic perspectives: (1) catalysts' structural design that can create pore sites and a confined environment and (2) electrode surface engineering with functional layers that can modify the electrode wettability and reactivity.

3.2.1 Structural design of catalysts

The strategy of designing a catalyst structure to regulate the local microenvironment is mainly achieved by elongating the

diffusion path from the bulk to the active sites. Consequently, the quantity of H^+ reaching the surface per unit time will be reduced, while K^+ and OH^- near the active sites will have more time to stay, ensuring a locally elevated pH and K^+ concentration microenvironment. For instance, by encapsulating or enclosing the catalytically active sites within an outer nanoshell or cage, designed as a core–shell structure, the local OH^- can be confined within the catalytic environment, while the bulk H^+ encounters greater resistance in reaching the catalyst. Consequently, it results in an elevation of the local microenvironment pH. Liu *et al*. [60] demonstrated that by encapsulating the Ni_5/NCS catalyst with N-doped carbon spheres, the resulting spatial confinement effect leads to a higher local microenvironment pH near the active sites. This phenomenon resulted in an approximately 20% increase in the FE_{CO} at 0.8 V (*vs*. RHE). Simultaneously, the introduction of hydrophobic nanoshells/cages increases the CO_2/H_2O ratio in the local microenvironment, thus suppressing the competitive discharge of H_2O (Figure 4a) at the electrode surface and enhancing the activity of the CO_2RR [61].

Introducing a porous structure on the catalyst surface is also one of the ways to increase the diffusion pathway. The length and diameter of the pores are two crucial parameters. With increasing pore length, the diffusion distance is further increased. However, it is worth noting that it also introduces additional ohmic loss, resulting in a decrease in the electrochemical active surface area (ECSA)-normalized current [62]. Decreasing the pore size hinders the transport of H^+ and restricts OH^-. Moreover, smaller pore sizes and deeper cavities can reduce the swirling velocity of ions on the surface, thereby increasing the residence time of intermediates (*e.g.*, *CO) and K^+. For example, compared with the $Cu_{0.9}Zn_{0.1}$ catalyst with a pore size of 150 nm, the catalysts with a pore size of 30 nm exhibit a higher C_2H_4 yield. Furthermore, the amplified electric field near the pore sites captures more K^+ in the pores to stabilize the intermediates. With the electrochemical hydrodynamic simulation during the electrolysis, the ionic vortex velocity generated in 30 nm pores is milder than that in the 150 nm pores or smaller pores (Figure 4b) [58]. The lower hydrodynamic velocity around the electrodes yields accumulated K^+ and OH^- concentrations. Similar strategies were applied by Ma *et al* [63]. The as-prepared Cu-based porous nanosheet presents an unprecedented C_{2+} performance in strongly acidic electrolytes (pH<1) with H_2 greatly suppressed, delivering a Faradaic efficiency of 83.7%±1.4% (Figure 3c) and partial current density of 0.56±0.02 A cm^{-2} accompanied by a high single-pass carbon efficiency (SPCE) of 54.4% and excellent stability over 150-h continuous operation. From COMSOL multiphysics finite-element-based simulations, the normalized potassium concentration based on the ECSA on porous

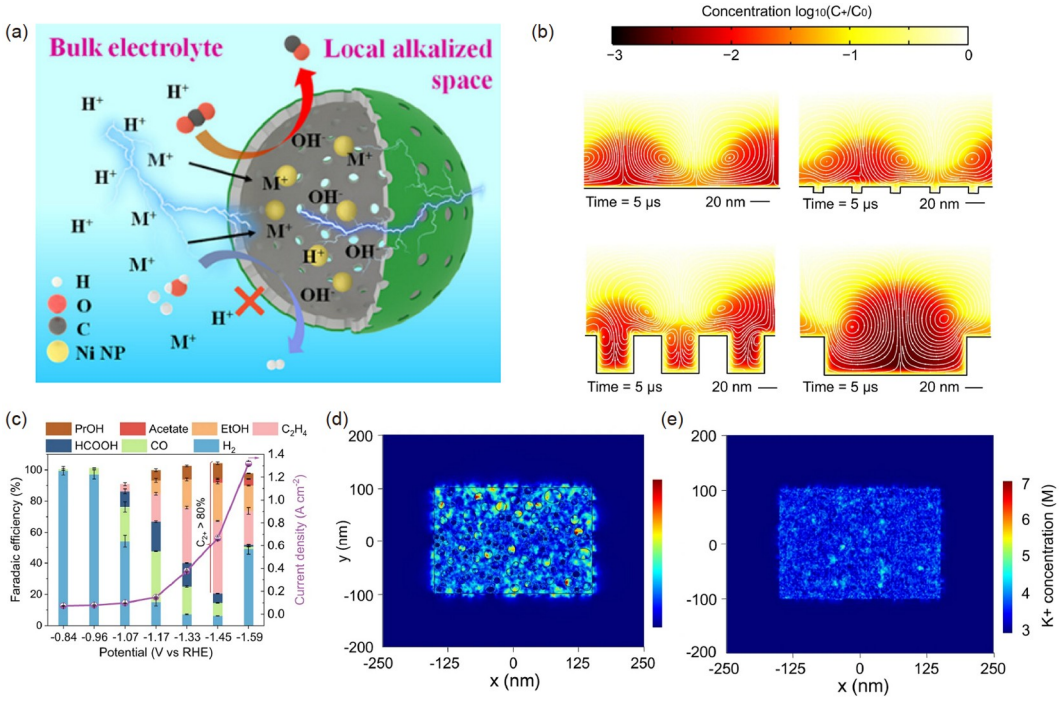

Figure 4 (a) pH environment and ions transporting around the hydrophobic nanoshell structure around the Ni_5@NCN catalyst. Reproduced with permission from [60]. Copyright 2022 American Chemical Society. (b) Simulated ion concentrations and electrokinetic flows near the planar and nanoporous (10, 30, and 150 nm) $Cu_{0.9}Zn_{0.1}$ surfaces. The white lines show the electrokinetic fluctuating vortex. Reproduced with permission from [58]. Copyright 2023 Springer Nature. (c) The product distribution of porous CuO in strong acid media at different applied potentials. The associated K^+ distribution on porous-CuO NS (d) and flat CuNS (e) models is obtained from COMSOL multiphysics finite-element-based simulations. Reproduced with permission from [63]. Copyright 2022 Springer Nature (color online).

nanostructured copper films (ER-CuSN) is 4.5 times higher than that on flat copper films (F-CuNS) (Figure 4d and 4e). Therefore, the intrinsic activity for C_{2+} production on ER-CuSN catalysts is much higher than that on F-CuNS catalysts. Currently, strategies such as electrochemical reduction of oxides, etched electrodes, and electrochemical displacement are important approaches for fabricating porous structures.

Reducing the diffusion of H^+ toward the microenvironment around the active sites can also be achieved through two other challenging approaches. The first approach involves directly adjusting the diffusion coefficient of H^+. McCory *et al*. [64] utilized pyridinic residues in the outer coordination sphere of poly(4-vinyl pyridine) (P4VP) as proton relays, which effectively inhibited the proton transfer rate and, consequently, suppressed the HER. The second approach entails using auxiliary agents to adsorb H^+ and protect the active sites from being affected by H^+. Rutkowska *et al*. [65] employed WO_3 as a substrate for polycrystalline Cu, as WO_3 can adsorb local protons during the electroreduction process, leading to the formation of H_xWO_3, which in turn increases the activation energy barrier for the HER. Nevertheless, selecting appropriate additives is a highly challenging task, as it requires simultaneously controlling the proton transfer and ensuring that the catalytic activity remains unhindered. Currently, there is limited literature available on this subject, thus warranting further research and exploration.

3.2.2 *Surface modification layer*

Although creating a suitable microenvironment near catalysts can significantly enhance the performance of the CO_2RR in acid media, challenges still remain, limiting the potential scalability of this strategy. First, some sophisticated but fragile surface structures may be effective in the low current densities but may be damaged under industrial operation conditions. On the other hand, introducing highly concentrated potassium salts may be prohibitive for the commercialization, and the solubility of common potassium salts is inadequate. Furthermore, microenvironment modulation should be integrated into a complete electrolyzer with the low ohmic resistance as much as possible. In this way, developing novel modification layers that provide diverse microenvironments may overcome the above problems.

It has been established that the concentrations of three key species in the local microenvironment, namely OH^-, K^+, and CO_2, can directly influence the reaction activity of the CO_2 RR. Following the design approach mentioned above, introducing a modifying layer to extend the spatial diffusion distance remains feasible for increasing OH^- and K^+ in the microenvironment near the active sites. Indeed, the increase in the local CO_2 concentration is achieved by regulating the hydrophobicity of the covering layer. For example, when SnBi catalysts are covered with a porous SiC-Nafion^{TM} coating (Figure 5a), the porous structure of the coating ensures a locally high concentration of K^+ and improves the local microenvironment pH [66]. Additionally, based on Pourbaix diagrams, the formation of a Sn/SnO_2 layer can enhance the stability of the catalyst by preventing the dissolution and re-growth of Sn, which would otherwise lead to the catalyst deactivation under high pH conditions. Additionally, constructing 3D porous multichannel electrodes and uniformly dispersing the active components within them can be another strategy [67]. 3D electrodes prepared using polyphenylsulfone (PPSU) as a polymer exhibit finger-shaped channels and layered honeycomb pores. By virtue of the tortuosity and porosity of the polymer, the pH gradient around the electrode is amplified, yielding an ultra-high local pH microenvironment.

On the other hand, the polytetrafluoroethylene (PTFE) particle layer has been proven to modulate the hydrophobicity of catalysts to regulate the CO_2 in the microenvironment [68]. PTFE-modified Ni–N–C catalysts can maintain a highly stable solid–liquid–gas interfacial microenvironment and inhibit water intrusion [69]. Moreover, an appropriate amount of PTFE can reduce the effective resistance and capacitance of the diffusion layer, thereby increasing the mass transfer of CO_2. With abundant local CO_2 concentration, the modified catalysts present a current density of 100 mA cm^{-2} with nearly 100% Faradaic efficiency for CO production (FE_{CO}) for up to 36 h in a flow cell with pH=2 (H_2SO_4+1 mol L^{-1} Cs_2SO_4), while the unmodified catalyst decays to 57.4% FE_{CO} after only 13 h. Strong hydrophobicity contributes to an increase in the CO_2/H_2O ratio in the microenvironment. However, excessive hydrophobicity can hinder the transport of K^+ and OH^- dissolved in H_2O, which are essential for participating in reactions, consequently affecting the catalyst's activity.

Apart from utilizing the spatial effects and hydrophobicity regulation of the modifying layer in the microenvironment, Wang *et al*. [70] confined K^+ and OH^- within the microenvironment through electrostatic effects. As shown in Figure 5b, they sprayed a layer of XC72R carbon onto PTFE-coated sputtered Cu (referred to as C/Cu/PTFE). The porous carbon surface layer was also charged during the reduction process, accumulating K^+ in the internal electric double layer. These densely packed cations, in turn, attract and confine negative OH^- ions near the surface of the carbon nanoparticles, resulting in an $FE_{C_2H_4}$ of 64.5% at 300 mA cm^{-2} in a flow cell with pH=2 (H_2SO_4+0.5 mol L^{-1} K_2SO_4).

Surface modification can also be approached by constructing a transport-regulating layer that can manipulate the mass transfer of key species in the microenvironment. The key to this construction is utilizing chemical functional groups to control the diffusion capacity of H^+ and K^+ in the

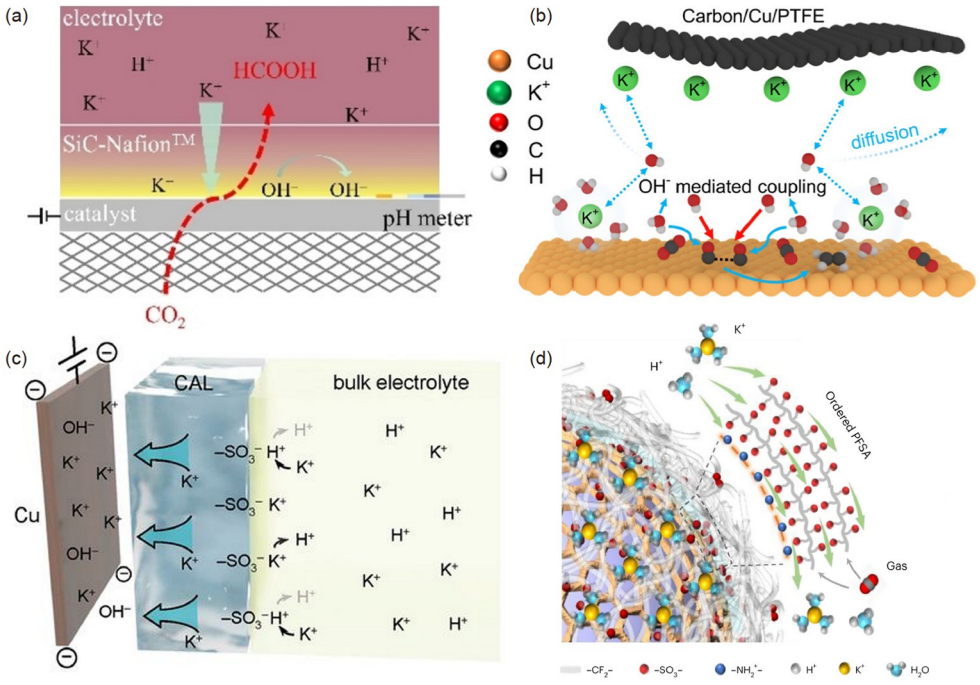

Figure 5 (a) Schematic of catalysts evenly coated by Nafion™ and undergoing CO_2RR in the pH 1 media. Reproduced with permission from [66]. Copyright 2023 John Wiley and Sons. (b) Schematic illustration of the *in-situ* confinement effect on OH^- for the carbon layer. Reproduced with permission from [70]. Copyright 2022 American Chemical Society. (c) Schematic illustration of the ionic environment and transport near the catalyst surface functionalized by the PFSA ionomer. Reproduced with permission from [13]. Copyright 2021 American Association for the Advancement of Science. (d) Schematic illustration of a functionalized COF particle for regulating ionomer structure and local ion and gas transport. Reproduced with permission from [74]. Copyright 2023 Springer Nature (color online).

bulk phase toward the active sites. This ensures a locally high pH and K^+ concentration in the microenvironment. As reported, *N*-methylpyridinium derivative films serve as additives that exhibit the capability to inhibit the HER and enhance the local CO_2/H_2O concentration ratio in alkali media [71]. The electrochemical deposition of *N*-methylpyridinium cations on Cu electrodes leads to a smaller plateau current density in hydrogen evolution (0.1 mol L^{-1} $KClO_4/HClO_4$ and pH≈2.2) compared with bare Cu, indicating the suppression of H^+ transport [72]. The inhibitory ability increases with the incrasing modifier concentration within the experimental range. Efficient conversion of CO_2 to C_{2+} products with >70% Faradaic efficiency can be achieved at pH=2 (H_3PO_4/KH_2PO_4) and low potassium-ion concentration ($[K^+]$=0.1 mol L^{-1}). However, the mechanism behind H^+ transport inhibition has not yet been fully elucidated, and the mechanical stability of the deposited films is not satisfactory.

During a long period of operation under alkali or neutral electrolytes, K^+ always runs off to generate solid precipitation, such as $KHCO_3$ and $K_4H_2(CO_3)_3\cdot 1.5H_2O$, blocking gas diffusion channels [73]. Integrating concentrated K^+ into an ionomer is a potential solution to anchor K^+ on the surface of the electrode. Huang *et al*. [13] proposed an ingenious perfluorosulfonic acid (PFSA), composed of tetrafluoroethylene and sulfonyl fluoride vinyl ether, exhibiting the excellent affinity for K^+ ions and serving as an ion-enhancing layer to enrich K^+ on the electrode surface (Figure 5c). When a mixture of PFSA and carbon nanospheres is used as a modifier for sputtered Cu on PTFE, XPS analysis confirms an increased local K^+ concentration, thereby enhancing the electrochemical coupling with specific intermediates and increasing the Faradaic efficiency of C_2H_4 production. Under a continuous operation at a current density of 1.2 A cm^{-2}, no evidence of K^+ precipitate formation was observed by in-depth XPS, indicating the ionomer successfully sustained K^+ rather than running off during the electrolysis.

It is worth noting that the disordered structure of PFSA can lead to a scattered distribution of ion channels, which may result in excessively high local H^+ concentrations and hinder the diffusion of local anionic and gaseous products, thereby suppressing the CO_2RR activity. To ensure the uniform distribution of PFSA, Zhao *et al*. [74] first covered polystyrene nanospheres (PS) with an acid-resistant covalent organic framework (COF) containing imine and carbonyl groups. In acidic environments, imine groups are positively charged, while the carbonyl groups can isomerize into negatively charged centers during the electroreduction to enrich K^+. Consequently, the imine groups form stable electrostatic pairs with $-SO_3^-$. Meanwhile, the hydrophobic fluorocarbon ($-CF_2-$) skeleton forms directed hydrophobic channels to ensure the stable discharge of gases as shown in Figure 5d.

The Cu electrode modified with this PS/COF/PFSA trilayer structure exhibits the significant suppression of competing HER (FE<15%) and improved CO_2RR selectivity (FE>85%) within the range of 100–400 mA cm^{-2}. Additionally, the content ratio of PFSA also has a significant influence on CO_2RR. A low content does not strongly restrict H^+ transport, resulting in increased HER, while a high content slows down the transfer rate of K^+ ions to the surface due to their strong affinity for abundant $–SO_3^-$. Therefore, the content of the modifier should be balanced to achieve optimal catalytic performance.

4 Electrolyzers for acidic CO_2RR

In addition to the development of electrocatalysts and the tuning of their reaction microenvironment, the reactor design is equally crucial for achieving high-performance CO_2RRs in acid. As we have elucidated the essential role of the cation effect, the H^+ concentration and the local pH on the acid CO_2RR performance in the Section 2, the parameters of an electroreactor, namely, the reactor configuration, the membrane and the electrolyte type, as well as the operation condition are highly important as they directly or indirectly affect the microenvironment of catalysts. Currently, three types of electroreactors have been employed for the CO_2RR in acid: H cells, flow cells, and membrane electrode assembly (MEA). In this section, we briefly review the recent advances in the design and optimization of electroreactors, with the special focus on MEA for the CO_2RR in acid, and provide some perspectives and suggestions for future research directions in this field.

The H cells are the simplest and most common type of electroreactors for CO_2RRs. The CO_2 gas is bubbled into the cathode compartment, where it participates in the reduction reaction on the catalyst surface. The merits of the H cell are its simplicity, low cost, easy operation, and flexibility in operation. Nevertheless, the mass transport of CO_2 and H_2O to the cathode is limited by the low solubility and diffusivity of CO_2 in aqueous electrolytes, resulting in low current density and CO_2 utilization. Moreover, the potential of its practical use is also plagued by its batch operation mode and low space-time yield [75].

To overcome these disadvantages, flow cells have been developed by incorporating a gas diffusion electrode or a gas diffusion layer, which can enhance mass transfer by creating a gas–liquid–solid interface. The CO_2 gas and the electrolyte are constantly supplied into the gap from one end and flow along the electrodes under a pressure gradient, warranting continuous operation. Compared with the H cell, the flow cell can deliver a much higher current density by increasing the gas flow rate, reducing the gap width, or applying a high pressure. Currently, the optimization of the flow cells for the CO_2RR in acid is mainly concentrated on the electrolyte management and gas-diffusion electrode engineering. This has been illustrated well by Sargent *et al*. [13], who utilized an electrolyte comprising a high-concentration of potassium cations and introduced a cation augmentation layer on the Cu electrode to boost the CO_2RR toward C_{2+} products.

Featuring a compact and scalable structure, MEA is a newly emerging and novel electroreactor for CO_2RR that has been inspired by proton-exchange membrane fuel-cell technology. It consists of an ion-exchange membrane sandwiched between two catalyst layers and two gas diffusion layers, where CO_2 gas and water vapor are supplied to the back side of the cathode. In the MEA electrolyzer, the zero-gap design (Figure 6a) reduces the ohmic resistance and results in the higher efficiency. As humidified CO_2 gas is supplied on the cathode side, it ameliorates the challenges of flooding encountered in H cell and flow cell systems. However, for anion-exchange membrane electrolysers (AEMMEAs), the local alkali environment at the cathode generates a considerable amount of (bi)carbonate ions, which are then exchanged to the anode through the AEM, leading to a further decrease in SPCE [75]. This problem can be circumvented by employing cation-exchange membranes or bipolar membranes in the acid-based MEA. To further improve the selectivity and carbon utilization efficiency of the CO_2RR in MEA, two other structures of MEA were designed: buffered MEA with modified layers and MEA used for CO_2 capture and regeneration (Figure 6b and 6c).

In a zero-gap MEA, the electric double layer (EDL) formed on the cathode surface becomes the direct reaction layer, and the OH^- ions and cations within the EDL directly impact the activity of the MEA. The cations in the anolyte will migrate to the cathode due to the electroosmosis in MEA cells, and can optimize the activity of the CO_2 reduction reaction at the cathode. By tuning the cations in the anolyte, the catalytic performance on the cathode can be regulated by the migrated cations accordingly. For example, by adjusting the amounts of H^+ and K^+ in the anolyte, Pan *et al*. [15] achieved an FE_{CO} of ~80%, an SPCE of ~90%, and stability for 50 h at 60 mA cm^{-2} in an Ag-based cation-exchange membrane MEA under the optimal condition of an anolyte of 0.01 mol L^{-1} H_2SO_4+0.01 mol L^{-1} Cs_2SO_4 (Cs^+:H^+=1:1). This strategy was also validated in a CEMMEA with the Ni–N–C catalysts as the cathode [48]. In the case of a bipolar membrane MEA, Burdyny *et al*. [76] adopted magnetron-sputtered Ag as the cathode and adjusted the concentration of KOH in the anolyte from 1 mol L^{-1} to 3 mol L^{-1}, resulting in a selectivity increase of cathodic CO to 68% at 50 mA cm^{-2}. Nevertheless, there exists a volcano relationship between activity and cation concentration (Figure 6d) because, under high-concentration conditions, the aggregation of alkali metal cations may lead to more precipitation of carbonates and bicarbonates, which hinder the transport of gaseous re-

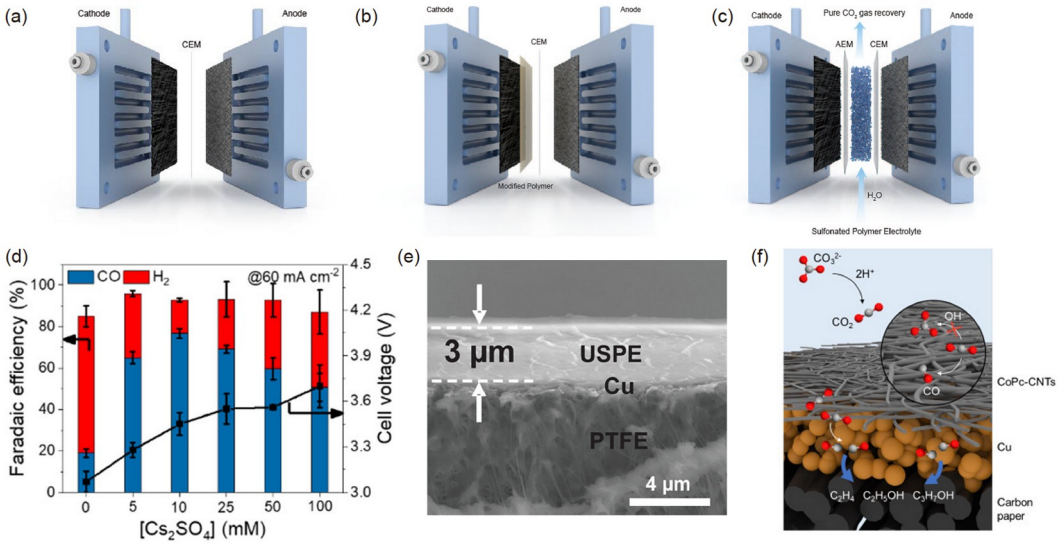

Figure 6 (a) Schematic illustration of an ordinary MEA reactor. (b) Schematic illustration of the MEA reactor with a modified polymer layer over the cathode. (c) Schematic illustration of the MEA reactor with a solid porous electrolyte for the CO_2 recycling. (d) FE_{CO} variation trend with the change in Cs_2SO_4 concentration at 60 mA cm^{-2} (at a fixed H_2SO_4 concentration of 10 mmol L^{-1}, CO_2 flow rate of 40 sccm), indicating a volcano-like performance in varied Cs^+. Reproduced with permission from [15]. Copyright 2022 American Chemical Society. (e) Cross-sectional SEM image of USPE-50 over the Cu/PTFE electrode. Reproduced with permission from [77]. Copyright 2023 John Wiley and Sons. (f) Illustration of the improved catalyst depositing a CoPc–CNT layer onto a Cu electrocatalyst. The CO_3^{2-} in the solvent *in-situ* generated CO_2 in the acidic microenvironment and was converted to organic products. Reproduced with permission from [84]. Copyright 2023 Elsevier Inc (color online).

actants and block the active sites on the catalyst surface, suppressing the CO_2RR. The concentration of OH^- must also be controlled within a reasonable range, as excessively high OH^- concentrations can lead to a decrease in SPCE due to the generation of CO_3^{2-} or HCO_3^-.

Alternatively, electrode membrane engineering has arisen as a strategy to tackle the trade-off between salt precipitation and the cation enhancement effect in MEAs. In this context, this can be achieved *via* the surface modification of catalysts or incorporating cations in the membrane. In a representative work, Adnan *et al*. [77] deposited a certain amount of Nafion on Cu to form an ultrathin solid polymer electrolyte (Figure 6e), to adjust the migration of K^+ and CO_3^{2-}, and suppress the water uptake and cathode flooding, thereby enhancing the CO_2RR performance. They also constructed a cation-embedded solid polymer electrolyte (CISPE), which was prepared by implanting cations during the Nafion deposition, to modulate the water flux and K^+ migration to the cathode. The results showed that increasing the K^+ loading in the ultrathin solid polymers improves the FE of gas products (*i.e*., CO and C_2H_4) while significantly decreasing the FE of H_2 significantly. Impressively, using an optimized CISPE membrane electrolyte and 1 mol L^{-1} KOH anolyte, a 90% selectivity toward CO_2 reduction products at 200 mA cm^{-2} was achieved, with a partial current density of 112 mA cm^{-2} toward C_2H_4.

In a typical MEA, direct contact with a cation-exchange membrane or bipolar membrane in a reversed bias mode can lead to an extremely low pH at the cathode surface, thereby promoting the HER. Therefore, one approach to enhance the pH is by adding a buffering layer between the cathode and the CEM. A weak cation-exchange layer consisting of a poly (allylamine hydrochloride) (PAH)/poly(acrylic acid) (PAA) bilayer grown on the surface of a bipolar membrane (BPM) cation-exchange layer (CEL) can rapidly increase the pH from 2 to 5 at the electrode surface (~20 nm). Compared with an unmodified BPMMEA with an FE_{CO} efficiency of less than 20%, this layer-by-layer assembly structure can enhance the FE_{CO} to 40% or higher [78]. Other approaches include using H_2O- or $NaHCO_3$-impregnated support layers [79] or anion-exchange materials as buffering layers, which also increase the electrode surface pH [80]. In these cases, the electrode surface pH becomes alkaline, which is nevertheless conducive to boosting the CO_2 reduction.

As another outlet, the configuration design of the MEA with a gap layer can also be utilized for carbon capture and recycling, which enables a carbon-efficient CO_2RR. For example, Xie *et al*. [81] employed a stationary unbuffered catholyte layer between the BPM and the cathode to promote C_{2+} products while ensuring that the (bi)carbonate is converted back, *in situ*, to CO_2 near the cathode. By developing a model that enables the design of the catholyte layer, they found that limiting the diffusion path length of reverted CO_2 to ~10 μm balances the CO_2 diffusion flux with the regeneration rate. As a result, a single-pass CO_2 utilization of 78%, which lowers the energy associated with the downstream separation of CO_2 by 10 times compared with past systems was achieved. Such a design can also be extra-

polated to the direct electrochemical upgrade of carbonates. For instance, Lee *et al*. [84] developed an MEA cell reactor comprised of an interposer and a Cu/CoPc–CNT-based electrocatalyst, where the interposer is a porous carbon paper coated with Nafion, which acts as a proton conductor and a physical barrier between the cathode and the anode. By virtue of the special acidic microenvironment, the authors direct the electrolysis of K_2CO_3 solution to achieve hydrocarbon generation rather than traditional gaseous CO_2, as shown in Figure 6f. To trigger this process, they adjusted the catalyst spacing to attain the desired conditions of low pH at the cation-exchange layer for *in-situ* CO_2(g) generation and [CO_2(g)]>4 vol% at the catalyst layer. Remarkably, this work exhibits 47% C_{2+} Faradaic efficiency at 300 mA cm^{-2} and a full cell voltage of 4.1 V with complete CO_2 utilization and high carbon efficiency.

5 Summary and outlook

The CO_2RR in acidic media offers us a tantalizing prospect to resolve the formation and crossover of carbonates in previous CO_2RR research, which used to be the bottleneck for its scalable application. Under the guidance of theoretical analysis, we take a comprehensive look at current strategies that can boost the energy efficiency for the acidic CO_2RR, including the fine-tuning of the formation of intermediates, manipulation of the surface microenvironment and optimization of the acidic electrolyzers. Despite the great effort put into acidic CO_2RR, several limitations and challenges cannot be overlooked before the commercialization.

(1) Although some well-designed catalysts that can attain remarkable selectivity toward target products even at the industrial current density for the CO_2RR have been reported, the lion's share of the product distribution remains concentrated on C_1 molecules. In contrast to the studies in alkali, converting CO_2 into single C_{2+} chemicals in acidic media is still a daunting task. This result accentuates the predicament that only Cu-based catalysts will display a notable but diversified C_{2+} selectivity [85,86], while in acidic media the predominant HER further hampers the generation of C_{2+} products. Furthermore, the stability of the catalyst should also be addressed in the future. Given that the corrosion effect is more pronounced in strong acid, some unstable components in catalysts may gradually leach out, resulting in deactivation. This issue has been addressed by Fan *et al*. [87] who employed the chelating effect to stabilize active Cu sites under an acidic electroreduction process. With the decoration of ethylenediaminetetraacetic acid among copper phthalocyanine (CuPc), both the X-ray photoelectron spectroscopy and *in-situ* X-ray absorption fine structure indicated a higher preservation ratio of Cu–N sites compared with bare CuPc. This modification exhibits the better stability for CO_2-to-CH_4 conversion under acidic media. The following studies may be encouraged for the direct observation of the true active sites during acidic CO_2 RR. With the assistance of *in-situ* characterizations, such as *in-situ* Raman, *in-situ* ATR-SEIRA spectra and *in-situ* X-ray absorption fine structure, elucidating potential countermeasures to enhance the intrinsic stability in acidic media will be feasible.

(2) As mentioned in the previous sections, the current acidic CO_2RR heavily relies on the excess concentration of alkali metal ions (typically 3 mol L^{-1}). However, this poses a serious challenge as the high concentration of cations will degrade the OER performance in the anode and cause the severe salt precipitation blocking the gas channels in the GDE. Therefore, developing a cation-free electrolyte for the acidic CO_2RR is the key scientific crux that needs to be addressed in future research. At present, two potential strategies are emerging to solve this problem. Specifically, the innovative cation-augmenting layer conceived by Sargent's group offers a promising way to trap K^+ around the surface of the cathodes. This system effectively prevents the K^+ depletion phenomenon that could lead to the salt precipitation or anode deterioration. Furthermore, elevating the local pH is another viable solution. In the Section 3.2, some ingenious designs are shown to accelerate the proton depletion near cathodes, including porous structure, organic layer modification or hydrophobicity modulation. These strategies have also been extensively studied in neutral CO_2RRs to enhance the local OH^- concentration, which could be readily extended to acidic CO_2RRs. To capture the pH gradient variation by the microenvironment modification, a reliable and convenient characterization technique is indispensable. Currently, pH gradients in the microenvironment are mostly simulated using the Poisson–Nernst–Planck equation. To gain a deeper understanding of the microscopic performance of acidic CO_2RRs, it is crucial to explore more direct methods such as molecular fluorescence probes to quantify pH gradients. Apart from its role in increasing local pH, K^+ also serves to enhance the electric field intensity of the EDL and stabilize intermediates. These functions can potentially be replaced by organic modification layers [82,83]. This opens up new possibilities for designing modification layers that can operate effectively at low alkali metal cation concentrations while achieving high current, activity, and stability.

(3) The optimization of acidic electrolyzers still has a long way to go. In the flow cell reactor, the CO_2 loss problem has not been perfectly resolved in some cases. Although the low pH inhibits the crossover of CO_3^{2-} to the anode side, the regenerated CO_2 bubbles may accumulate between the catalysts and membrane rather than return to the gaseous chamber. This phenomenon can introduce extra ohmic resistance accounting for the undesirable energy loss. Hence,

employing the electrode engineering to design bubble-free electrodes can be an appealing method. Another effective strategy to recover CO_2 from electrolytes is applying porous solid electrolytes proposed by Wang and colleagues [88]. By incorporating an acidic buffer layer between electrodes, the crossover carbonates will be neutralized and released in the form of pure CO_2. The MEA reactor demonstrates higher energy efficiency than the flow cell reactor, whereas the potential degradation of the membrane lifetime is also alarming [73]. Therefore, membrane electrode engineering is essential to improve the durability and performance of the electrolyzer while suppressing the parasitic HER.

(4) Industrial prospects still face significant challenges. Despite the vigorous development of CO_2RR in the past decades, further progress is still required for the large-scale production. Martin *et al*. [89] thoroughly calculated the required parameters to commercialize CO_2RR. To make the whole process economical, the threshold current density is beyond 200 mA cm^{-2}, and the FE for C_{2+} products should be over 80%. For stability, the whole electrolyzer should constantly operate for more than 5,000 h with an overpotential lower than 0.4 V for practical applications. Additionally, the full cell energy conversion efficiency should surpass 60% [90]. To efficiently operate acidic CO_2RRs, special obstacles hamper their commercialization. First, the excess concentration of K^+ results in severe salt precipitation and rapid performance degradation. Introducing the cation-augmentation layer may be a promising solution. However, the surface modification layers and catalyst structure designs adopted to reduce the K^+ concentration can lead to voltage losses, especially when dealing with surface coatings. When the coating layer is too thin, it faces mechanical strength and chemical stability challenges in acidic environments. By contrast, the thick layer results in significant contact resistance and cell pressure losses. Therefore, selecting an appropriate surface coverage layer is crucial. Additionally, the corrosive and harsh acidic environments, along with the industrial requirements for long and efficient operation (>100 mA cm^{-2}, >2,000 h), inevitably result in the equipment erosion, membrane detachment, and performance deterioration of the active materials [91,92].

In summary, the acidic CO_2RR presents an enticing opportunity to significantly enhance the single-pass conversion efficiency for CO_2 valorization. By circumventing the additional costs associated with the CO_2 separation and recovery, this technique holds the promise for practical industrial-scale applications in the future. Although considerable progress has been made in exploring innovative catalysts, electrolytes, and electrolysers in recent decades, the challenge of achieving scalable acidic CO_2RR persists, particularly in terms of operational stability and energy efficiency, as highlighted in this review. Nevertheless, we remain optimistic because continuous research and advancements in the catalyst development and electrolyzer optimization will soon bring to fruition in the vision of utilizing renewable energy to upcycle CO_2 from the atmosphere.

Acknowledgements C.X. acknowledges the National Key Research and Development Program of China (2022YFB4102000), NSFC (22102018 and 52171201), the Natural Science Foundation of Sichuan Province (2022NSFSC0194), the "Pioneer" and "Leading Goose" R&D Program of Zhejiang (2023C03017), the Huzhou Science and Technology Bureau (2022GZ45), the Hefei National Research Center for Physical Sciences at the Microscale (KF2021005), and the University of Electronic Science and Technology of China for startup funding (A1098531023601264). T.Z. acknowledges the NSFC (22278067 and 22322201), the Natural Science Foundation of Sichuan Province (2023NSFSC0094) and the University of Electronic Science and Technology of China for startup funding (A1098531023601356).

Conflict of interest The authors declare no conflict of interest.

1 Canadell JG, Le Quéré C, Raupach MR, Field CB, Buitenhuis ET, Ciais P, Conway TJ, Gillett NP, Houghton RA, Marland G. *Proc Natl Acad Sci USA*, 2007, 104: 18866–18870
2 Jin S, Hao Z, Zhang K, Yan Z, Chen J. *Angew Chem Int Ed*, 2021, 60: 20627–20648
3 Zheng T, Liu C, Guo C, Zhang M, Li X, Jiang Q, Xue W, Li H, Li A, Pao CW, Xiao J, Xia C, Zeng J. *Nat Nanotechnol*, 2021, 16: 1386–1393
4 Dinh CT, Burdyny T, Kibria MG, Seifitokaldani A, Gabardo CM, García de Arquer FP, Kiani A, Edwards JP, De Luna P, Bushuyev OS, Zou C, Quintero-Bermudez R, Pang Y, Sinton D, Sargent EH. *Science*, 2018, 360: 783–787
5 Li F, Thevenon A, Rosas-Hernández A, Wang Z, Li Y, Gabardo CM, Ozden A, Dinh CT, Li J, Wang Y, Edwards JP, Xu Y, McCallum C, Tao L, Liang ZQ, Luo M, Wang X, Li H, O'Brien CP, Tan CS, Nam DH, Quintero-Bermudez R, Zhuang TT, Li YC, Han Z, Britt RD, Sinton D, Agapie T, Peters JC, Sargent EH. *Nature*, 2020, 577: 509–513
6 Fan L, Liu CY, Zhu P, Xia C, Zhang X, Wu ZY, Lu Y, Senftle TP, Wang H. *Joule*, 2022, 6: 205–220
7 Gao D, Arán-Ais RM, Jeon HS, Roldan Cuenya B. *Nat Catal*, 2019, 2: 198–210
8 Kibria MG, Edwards JP, Gabardo CM, Dinh CT, Seifitokaldani A, Sinton D, Sargent EH. *Adv Mater*, 2019, 31: 1807166
9 Chen C, Li Y, Yang P. *Joule*, 2021, 5: 737–742
10 Rabinowitz JA, Kanan MW. *Nat Commun*, 2020, 11: 5231
11 Ozden A, de Arquer FPG, Huang JE, Wicks J, Sisler J, Miao RK, O'Brien CP, Lee G, Wang X, Ip AH, Sargent EH, Sinton D. *Nat Sustain*, 2022, 5: 563–573
12 Kim JYT, Zhu P, Chen FY, Wu ZY, Cullen DA, Wang H. *Nat Catal*, 2022, 5: 288–299
13 Huang JE, Li F, Ozden A, Rasouli AS, de Arquer FPG, Liu S, Zhang S, Luo M, Wang X, Lum Y, Xu Y, Bertens K, Miao RK, Dinh CT, Sinton D, Sargent EH. *Science*, 2021, 372: 1074–1078
14 Monteiro MCO, Philips MF, Schouten KJP, Koper MTM. *Nat Commun*, 2021, 12: 4943
15 Pan B, Fan J, Zhang J, Luo Y, Shen C, Wang C, Wang Y, Li Y. *ACS Energy Lett*, 2022, 7: 4224–4231
16 Cao Y, Chen Z, Li P, Ozden A, Ou P, Ni W, Abed J, Shirzadi E, Zhang J, Sinton D, Ge J, Sargent EH. *Nat Commun*, 2023, 14: 2387
17 Li X, Zhang P, Zhang L, Zhang G, Gao H, Pang Z, Yu J, Pei C, Wang T, Gong J. *Chem Sci*, 2023, 14: 5602–5607
18 Xie Y, Ou P, Wang X, Xu Z, Li YC, Wang Z, Huang JE, Wicks J, McCallum C, Wang N, Wang Y, Chen T, Lo BTW, Sinton D, Yu JC, Wang Y, Sargent EH. *Nat Catal*, 2022, 5: 564–570
19 Gabardo CM, O'Brien CP, Edwards JP, McCallum C, Xu Y, Dinh CT,

Li J, Sargent EH, Sinton D. *Joule*, 2019, 3: 2777–2791
20 Chen X, Chen J, Alghoraibi NM, Henckel DA, Zhang R, Nwabara UO, Madsen KE, Kenis PJA, Zimmerman SC, Gewirth AA. *Nat Catal*, 2021, 4: 20–27
21 Ni J, Cheng Q, Liu S, Wang M, He Y, Qian T, Yan C, Lu J. *Adv Funct Mater*, 2023, 33: 2212483
22 Moreno-García P, Kovács N, Grozovski V, Gálvez-Vázquez MJ, Vesztergom S, Broekmann P. *Anal Chem*, 2020, 92: 4301–4308
23 Ooka H, Figueiredo MC, Koper MTM. *Langmuir*, 2017, 33: 9307–9313
24 Bondue CJ, Graf M, Goyal A, Koper MTM. *J Am Chem Soc*, 2021, 143: 279–285
25 Kim C, Bui JC, Luo X, Cooper JK, Kusoglu A, Weber AZ, Bell AT. *Nat Energy*, 2022, 7: 116
26 Monteiro MCO, Dattila F, Hagedoorn B, García-Muelas R, López N, Koper MTM. *Nat Catal*, 2021, 4: 654–662
27 Gu J, Liu S, Ni W, Ren W, Haussener S, Hu X. *Nat Catal*, 2022, 5: 268–276
28 Qin HG, Li FZ, Du YF, Yang LF, Wang H, Bai YY, Lin M, Gu J. *ACS Catal*, 2022, 13: 916–926
29 Zhang F, Co AC. *Angew Chem Int Ed*, 2020, 59: 1674–1681
30 Wen G, Ren B, Zheng Y, Li M, Silva C, Song S, Zhang Z, Dou H, Zhao L, Luo D, Yu A, Chen Z. *Adv Energy Mater*, 2022, 12: 2103289
31 Wang Z, Hou P, Wang Y, Xiang X, Kang P. *ACS Sustain Chem Eng*, 2019, 7: 6106–6112
32 Lees EW, Mowbray BAW, Parlane FGL, Berlinguette CP. *Nat Rev Mater*, 2022, 7: 55–64
33 Fan L, Xia C, Yang F, Wang J, Wang H, Lu Y. *Sci Adv*, 2020, 6: eaay3111
34 Woldu AR, Huang Z, Zhao P, Hu L, Astruc D. *Coord Chem Rev*, 2022, 454: 214340
35 Nitopi S, Bertheussen E, Scott SB, Liu X, Engstfeld AK, Horch S, Seger B, Stephens IEL, Chan K, Hahn C, Nørskov JK, Jaramillo TF, Chorkendorff I. *Chem Rev*, 2019, 119: 7610–7672
36 Seh ZW, Kibsgaard J, Dickens CF, Chorkendorff I, Nørskov JK, Jaramillo TF. *Science*, 2017, 355: eaad4998
37 Lee CW, Yang KD, Nam DH, Jang JH, Cho NH, Im SW, Nam KT. *Adv Mater*, 2018, 30: 1704717
38 Shen J, Kortlever R, Kas R, Birdja YY, Diaz-Morales O, Kwon Y, Ledezma-Yanez I, Schouten KJP, Mul G, Koper MTM. *Nat Commun*, 2015, 6: 8177
39 Jiang Z, Zhang Z, Li H, Tang Y, Yuan Y, Zao J, Zheng H, Liang Y. *Adv Energy Mater*, 2022, 13: 2203603
40 Resasco J, Chen LD, Clark E, Tsai C, Hahn C, Jaramillo TF, Chan K, Bell AT. *J Am Chem Soc*, 2017, 139: 11277–11287
41 Liu H, Liu J, Yang B. *ACS Catal*, 2021, 11: 12336–12343
42 Xu Z, Sun M, Zhang Z, Xie Y, Hou H, Ji X, Liu T, Huang B, Wang Y. *ChemCatChem*, 2022, 14: e202200052
43 Goyal A, Koper MTM. *Angew Chem Int Ed*, 2021, 60: 13452–13462
44 Liu E, Li J, Jiao L, Doan HTT, Liu Z, Zhao Z, Huang Y, Abraham KM, Mukerjee S, Jia Q. *J Am Chem Soc*, 2019, 141: 3232–3239
45 Monteiro MCO, Dattila F, López N, Koper MTM. *J Am Chem Soc*, 2022, 144: 1589–1602
46 Jiao X, Hu Z, Li L, Wu Y, Zheng K, Sun Y, Xie Y. *Sci China Chem*, 2022, 65: 428–440
47 Varela AS, Kroschel M, Leonard ND, Ju W, Steinberg J, Bagger A, Rossmeisl J, Strasser P. *ACS Energy Lett*, 2018, 3: 812–817
48 Cave ER, Shi C, Kuhl KP, Hatsukade T, Abram DN, Hahn C, Chan K, Jaramillo TF. *ACS Catal*, 2018, 8: 3035–3040
49 Wang Y, Wang C, Wei Y, Wei F, Kong L, Feng J, Lu JQ, Zhou X, Yang F. *Chem Eur J*, 2022, 28: e202201832
50 Li H, Li H, Wei P, Wang Y, Zang Y, Gao D, Wang G, Bao X. *Energy Environ Sci*, 2023, 16: 1502–1510
51 Wu Q, Liang J, Han LL, Huang YB, Cao R. *Chem Commun*, 2023, 59: 5102–5105
52 Gonglach S, Paul S, Haas M, Pillwein F, Sreejith SS, Barman S, De R, Müllegger S, Gerschel P, Apfel UP, Coskun H, Aljabour A, Stadler P, Schöfberger W, Roy S. *Nat Commun*, 2019, 10: 3864
53 De R, Gonglach S, Paul S, Haas M, Sreejith SS, Gerschel P, Apfel UP, Vuong TH, Rabeah J, Roy S, Schöfberger W. *Angew Chem Int Ed*, 2020, 59: 10527–10534
54 Zhang L, Feng J, Liu S, Tan X, Wu L, Jia S, Xu L, Ma X, Song X, Ma J, Sun X, Han B. *Adv Mater*, 2023, 35: e2209590
55 Yang F, Elnabawy AO, Schimmenti R, Song P, Wang J, Peng Z, Yao S, Deng R, Song S, Lin Y, Mavrikakis M, Xu W. *Nat Commun*, 2020, 11: 1088
56 Qiao Y, Lai W, Huang K, Yu T, Wang Q, Gao L, Yang Z, Ma Z, Sun T, Liu M, Lian C, Huang H. *ACS Catal*, 2022, 12: 2357–2364
57 Shen H, Jin H, Li H, Wang H, Duan J, Jiao Y, Qiao SZ. *Nat Commun*, 2023, 14: 2843
58 Zhang J, Guo C, Fang S, Zhao X, Li L, Jiang H, Liu Z, Fan Z, Xu W, Xiao J, Zhong M. *Nat Commun*, 2023, 14: 1298
59 Bui JC, Kim C, King AJ, Romiluyi O, Kusoglu A, Weber AZ, Bell AT. *Acc Chem Res*, 2022, 55: 484–494
60 Liu Z, Yan T, Shi H, Pan H, Cheng Y, Kang P. *ACS Appl Mater Interfaces*, 2022, 14: 7900–7908
61 Fan Q, Bao GX, Chen X, Meng Y, Zhang S, Ma X. *ACS Catal*, 2022, 12: 7517–7523
62 Goyal A, Bondue CJ, Graf M, Koper MTM. *Chem Sci*, 2022, 13: 3288–3298
63 Ma Z, Yang Z, Lai W, Wang Q, Qiao Y, Tao H, Lian C, Liu M, Ma C, Pan A, Huang H. *Nat Commun*, 2022, 13: 7596
64 Liu Y, McCrory CCL. *Nat Commun*, 2019, 10: 1683
65 Rutkowska IA, Chmielnicka A, Krzywiecki M, Kulesza PJ. *ACS Meas Sci Au*, 2022, 2: 553–567
66 Li L, Liu Z, Yu X, Zhong M. *Angew Chem Int Ed*, 2023, 62: e202300226
67 Yan T, Pan H, Liu Z, Kang P. *Small*, 2023, 19: e2207650
68 Xing Z, Hu L, Ripatti DS, Hu X, Feng X. *Nat Commun*, 2021, 12: 136
69 Sheng X, Ge W, Jiang H, Li C. *Adv Mater*, 2022, 34: e2201295
70 Wang Z, Li Y, Zhao X, Chen S, Nian Q, Luo X, Fan J, Ruan D, Xiong BQ, Ren X. *J Am Chem Soc*, 2023, 145: 6339–6348
71 Han Z, Kortlever R, Chen HY, Peters JC, Agapie T. *ACS Cent Sci*, 2017, 3: 853–859
72 Nie W, Heim GP, Watkins NB, Agapie T, Peters JC. *Angew Chem Int Ed*, 2023, 62: e202216102
73 Sassenburg M, Kelly M, Subramanian S, Smith WA, Burdyny T. *ACS Energy Lett*, 2023, 8: 321–331
74 Zhao Y, Hao L, Ozden A, Liu S, Miao RK, Ou P, Alkayyali T, Zhang S, Ning J, Liang Y, Xu Y, Fan M, Chen Y, Huang JE, Xie K, Zhang J, O'Brien CP, Li F, Sargent EH, Sinton D. *Nat Synth*, 2023, 2: 403–412
75 Wakerley D, Lamaison S, Wicks J, Clemens A, Feaster J, Corral D, Jaffer SA, Sarkar A, Fontecave M, Duoss EB, Baker S, Sargent EH, Jaramillo TF, Hahn C. *Nat Energy*, 2022, 7: 130–143
76 Yang K, Li M, Subramanian S, Blommaert MA, Smith WA, Burdyny T. *ACS Energy Lett*, 2021, 6: 4291–4298
77 Adnan MA, Zeraati AS, Nabil SK, Al-Attas TA, Kannimuthu K, Dinh CT, Gates ID, Kibria MG. *Adv Energy Mater*, 2023, 13: 2203158
78 Yan Z, Hitt JL, Zeng Z, Hickner MA, Mallouk TE. *Nat Chem*, 2021, 13: 33–40
79 Salvatore DA, Weekes DM, He J, Dettelbach KE, Li YC, Mallouk TE, Berlinguette CP. *ACS Energy Lett*, 2018, 3: 149–154
80 O'Brien CP, Miao RK, Liu S, Xu Y, Lee G, Robb A, Huang JE, Xie K, Bertens K, Gabardo CM, Edwards JP, Dinh CT, Sargent EH, Sinton D. *ACS Energy Lett*, 2021, 6: 2952–2959
81 Xie K, Miao RK, Ozden A, Liu S, Chen Z, Dinh CT, Huang JE, Xu Q, Gabardo CM, Lee G, Edwards JP, O'Brien CP, Boettcher SW, Sinton D, Sargent EH. *Nat Commun*, 2022, 13: 3609
82 Fan M, Huang JE, Miao RK, Mao Y, Ou P, Li F, Li XY, Cao Y, Zhang Z, Zhang J, Yan Y, Ozden A, Ni W, Wang Y, Zhao Y, Chen Z, Khatir B, O'Brien CP, Xu Y, Xiao YC, Waterhouse GIN, Golovin K, Wang Z, Sargent EH, Sinton D. *Nat Catal*, 2023, DOI:10.1038/s41929-023-01003-5
83 Nam DH, De Luna P, Rosas-Hernández A, Thevenon A, Li F, Agapie

T, Peters JC, Shekhah O, Eddaoudi M, Sargent EH. *Nat Mater*, 2020, 19: 266–276
84 Lee G, Rasouli AS, Lee BH, Zhang J, Won DH, Xiao YC, Edwards JP, Lee MG, Jung ED, Arabyarmohammadi F, Liu H, Grigioni I, Abed J, Alkayyali T, Liu S, Xie K, Miao RK, Park S, Dorakhan R, Zhao Y, O'Brien CP, Chen Z, Sinton D, Sargent E. *Joule*, 2023, 7: 1277–1288
85 Kong X, Wang C, Zheng H, Geng Z, Bao J, Zeng J. *Sci China Chem*, 2021, 64: 1096–1102
86 Liu C, Gong J, Gao Z, Xiao L, Wang G, Lu J, Zhuang L. *Sci China Chem*, 2021, 64: 1660–1678
87 Fan M, Miao RK, Ou P, Xu Y, Lin ZY, Lee TJ, Hung SF, Xie K, Huang JE, Ni W, Li J, Zhao Y, Ozden A, O'Brien CP, Chen Y, Xiao YC, Liu S, Wicks J, Wang X, Abed J, Shirzadi E, Sargent EH, Sinton D. *Nat Commun*, 2023, 14: 3314
88 Zhu P, Wu ZY, Elgazzar A, Dong C, Wi TU, Chen FY, Xia Y, Feng Y, Shakouri M, Kim JY, Fang Z, Hatton TA, Wang H. *Nature*, 2023, 618: 959–966
89 Martín AJ, Larrazábal GO, Pérez-Ramírez J. *Green Chem*, 2015, 17: 5114–5130
90 De Luna P, Hahn C, Higgins D, Jaffer SA, Jaramillo TF, Sargent EH. *Science*, 2020, 364: eaav3506
91 Jin M, Zhang X, Niu S, Wang Q, Huang R, Ling R, Huang J, Shi R, Amini A, Cheng C. *ACS Nano*, 2022, 16: 11577–11597
92 Miller HA, Bouzek K, Hnat J, Loos S, Bernäcker CI, Weißgärber T, Röntzsch L, Meier-Haack J. *Sustain Energy Fuels*, 2020, 4: 2114–2133